

Influence of TiO₂ and SiO₂ as Additives to Improve Electrochemical Properties of MoS₂ as Anode Material for Lithium Ion Batteries

Beata Kurc*, Maciej Soltan

Institute of Chemistry and Electrochemistry, Faculty of Chemical Technology, Poznan University of Technology, Berdychowo 4, PL-60965 Poznan, Poland

*E-mail: beata.kurc@put.poznan.pl

Received: 4 January 2019 / Accepted: 14 February 2019 / Published: 10 April 2019

The paper attempts to dope the system containing MoS₂ in order to check the reversibility of the cell's operation. To this end, commercial TiO₂ and SiO₂ were used from emulsion systems. The electrochemical properties of the MoS₂/TiO₂ and MoS₂/SiO₂ composites were evaluated by cycling voltammetry (CV), charge-discharge cycles and impedance spectroscopy. The MoS₂/oxide composites exhibited high capacity and excellent cyclic stability used as anode materials for Li-ion batteries. The composite exhibited the highest reversible capacity (320 mAh g⁻¹) and excellent cyclic stability. After 80 cycles, it still retained 300 mAh g⁻¹. The significant improvements in the electrochemical properties of the MoS₂/TiO₂ and MoS₂/SiO₂ composites could be attributed to the graphene-like structure of the MoS₂ nanosheets and the synergistic effects of oxide-like MoS₂. The very good electrochemical performances of MoS₂/TiO₂ electrode originate from the purposely designed unique structures, in which the MoS₂ provide more lithium storage sites and the shorter Li-ion diffusion length, and the stability of capacity.

Keywords: MoS₂, TiO₂, SiO₂, galvanostatic charge–discharge, reversibility

1. INTRODUCTION

MoS₂ thermal stability is maintained to 1100 °C (in the case of highly oxidizing environments), but air can be reduced to 35-400 °C [1]. This relationship in some respects is similar to graphite. It is difficult to organoleptically distinguish between these two substances. They have a similar structure and color, plus sulphide as graphite, has a very low coefficient of friction. Natural low ionic and electron conductivity, volume expansion, pulverization, stress accumulation and unstable surface

contact between the electrolyte and the electrode surface, using MoS₂ as the anode material during the lithium insertion/deinsertion process, determines a rapid decrease in capacitance, and a small number of life cycles. To solve these problems, molybdenum sulphide with graphene (as an electrolyte paste) is synthesized by the solvothermal method and subsequently heat-treated. This results in a reversibility of 72-78 %. MoS₂ particles thus obtained have a spherical shape, providing a high availability of specific surface area, pore volume and flexible film formed of graphene. This leads to easier diffusion of electrolyte and lithium ions, creating a stable interstitial electrolyte-electrode, limiting volume expansion [2-12].

Industrial methods of TiO₂ synthesis are two: sulphate and chloride. Their names are derived from the salts used, of which titanium oxide (IV) is obtained. In the case of the sulphate method, it is titanyl sulfate, and chloride - titanium tetrachloride gas in the reaction of oxidation with pure oxygen at elevated temperature. The chemical industry uses two basic sources of titanium using these methods: ilmenite and the titanium route. Various products are obtained for different production technologies. Therefore, technical TiO₂ differ significantly (crystallographic form, surface treatment, properties and possible applications), depending on who produced them and how they were produced [13-15].

The intercalated composites of molybdenum sulphide and reduced graphene oxide (MoS₂/rGO) are synthesized using the hydrothermal method supported by silicon oxide (IV). SiO₂ nanoparticles act as a stabilizing agent for the surface structure of MoS₂ layers. As a result, there is no need to use other amorphous carbon precursors in the synthesis. Silicon oxide (IV) can also reduce the rate of lithium defects and compositions in the final product. The structure characteristics of the layered MoS₂/rGO composite show that molybdenum (IV) sulphide, consisting of one to four layers, has a tendency to peel. Nevertheless, it covers the structure of graphene evenly and precisely. The spacing between the layers of molybdenum sulphide (IV) is increased (0.7-1.17 nm). Electrochemical tests show that the composite provides high reversible capacity - 1260.6 mAh g⁻¹ in the first cycle and that it retains 94.9% capacity after 50 cycles [15].

The purpose of the work was to use molybdenum (IV) sulphide as a potential electrode material used in lithium-ion cells and to improve its electro-chemical properties (reversibility of charging/discharging processes) and to compare the obtained data with literature data. The scope of work included the determination of the percentage composition of electrodes (molybdenum sulfide (IV) and molybdenum sulphide (IV) with the addition of titanium oxide (IV) and silicon oxide (IV)), their preparation, assembly of the measurement system, familiarization with the operation of selected electrochemical techniques.

2. EXPERIMENTAL

2.1. Materials

There are used materials which are presented in Table 1.

Table 1. Proposed materials.

MATERIALS	SYMBOLS	PROCUCER
Molybdenum sulphide	MoS ₂	Sigma Aldrich
acetylen black	AB	Fluka
poly(vinylidene fluoride)	PVdF, $M_w=180\ 000$	Fluka
lithium foil	Li, 0.75 mm thick	Aldrich,
<i>N</i> -methyl-2-pyrrolidinone	NMP	Fluka
lithium hexafluorophosphate	LiPF ₆	Sigma Aldrich
titanium oxide	TiO ₂	Sigma Aldrich
ethylene carbonate	EC	Fluka
dimethyl carbonate	DMC	Fluka
Silica oxide	SiO ₂	[17]

Electrolytes were obtained by dissolution of solid LiPF₆ salt in liquid EC/DMC (1:1 v/v). The tested anodes were prepared on a copper foil (Hohsen, Japan) by a casting technique, from a slurry of MoS₂/TiO₂ or MoS₂/SiO₂, graphite and PVdF in NMP. The ratio of components was (electrode material – M) M:G:PVdF=70:20:10 (by weight). After evaporation of the solvent (NMP) at 120 °C in vacuum, a layer of the MoS₂/TiO₂ or MoS₂/SiO₂ (geometrical surface area was 1 cm²) electrode containing AB and binder (PVdF) was formed. Typically, the mass composition of the electrodes was as follows: Li: ca. 45 mg (0.785 cm²), MoS₂/TiO₂ or MoS₂/SiO₂: 2.5–3.5 mg.

Table 2. The ratio of components to prepare electrodes (by weight/ wt.%).

		Content / %		
		Active material	AB	PVdF
Electrode with silica oxide (IV)	5 wt.%	80	10	10
	10 wt.%	80	10	10
or				
Electrode with titanium oxide (IV)	20 wt.%	80	10	10

Based on the study and optimization of the composition of the electrodes, selected 3% in addition to the spinel MoS₂. After solvent (NMP) vacuum evaporation at 120 °C, a layer of the carbon electrode was formed, containing the active material (MoS₂), an electronic conductor (CB) and the binder (PVdF).

2.3. Procedures and measurements

The performance of the cells was characterized using galvanostatic charge–discharge tests, cyclic voltammetry (CV) and electrochemical impedance spectroscopy (EIS). It was described in

previously work [16]. The morphology of the TiO_2 , SiO_2 and MoS_2 (pristine and after electrochemical cycling) were observed under a scanning electron microscope (SEM, Tescan Vega 5153).

3. RESULTS AND DISCUSSION

3.1. The electrode based on pure MoS_2

Molybdenum disulphide occurs in two crystalline forms: hexagonal and rhombohedral. The hexagonal form is by far the most popular and is the only type of commercial ore mining. The hexagonal form of molybdenum disulphide was used in synthetic MoS_2 . The hexagonal form of MoS_2 is characterized by layers in which the molybdenum atoms have a triangular prismatic appearance and coordinate with six sulfur atoms, in which one flat, hexagonal layer of molybdenum atoms interweaves between the two layers of sulfur atoms. This metal sulfide is composed of three atom layers (S–Mo–S) stacked together through van der Waals interactions. Due to this layered structure, Li^+ ions can easily intercalate and exfoliate. Since the patent publication of the first lithium ion battery using MoS_2 , several different MoS_2 morphologies have been used in lithium ion batteries[18-20].

In order to characterize the structure of molybdenum sulphide (IV), scanning electron microscopy (SEM) was taken.

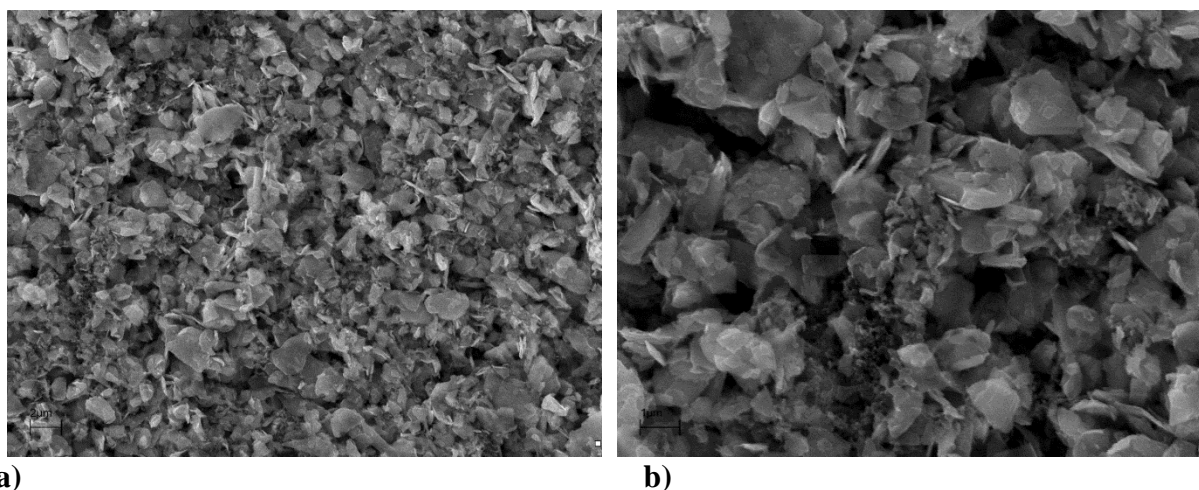


Figure 1. SEM of the pure MoS_2 anode (two magnification): a) 2 μm , and b) 1 μm

Figure 1 clearly explains the possibility of using MoS_2 as an electrode material. Its lamellar structure increases the specific surface (it is a macroporous material) and determines the occurrence of numerous spaces in which lithium ions can locate during insertion processes. As a result, the distance between layers of molybdenum sulphide is 0.6212 nm [21]. Considering the lithium ion radius, which is 0.059 nm, it is obvious that this compound can be considered as a potential electrode material [22].

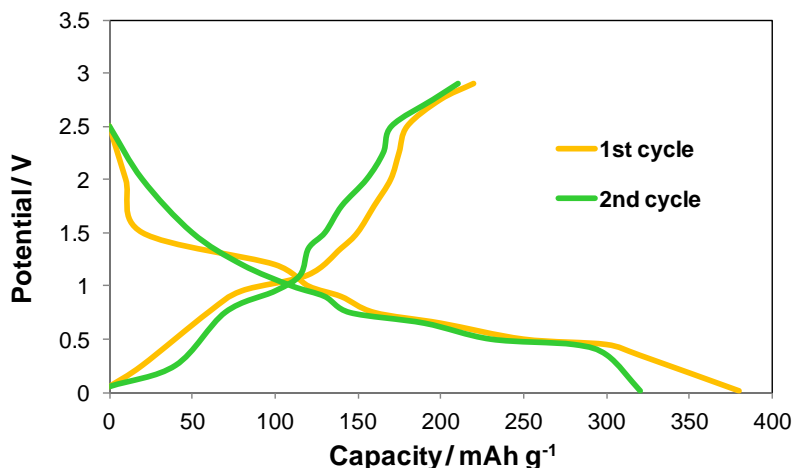


Figure 2. Discharge-charge profiles of selected cycles at current density 50 mA g^{-1} of $\text{MoS}_2|1\text{M LiPF}_6$ in EC/DMC|Li.

Figure 2 shows galvanostatic charging and discharging curves for electrodes with molybdenum sulphide (IV) without additives for two cycles of operation. From this graph it is clear that in the next cycle the material capacity drops from about 385 mAh g^{-1} to about 350 mAh g^{-1} in the insertion process, which gives a process reversibility of about 91%. Taking into account the loading and unloading within one cycle, the obtained capacities are not similar (insertion - 385 mAh g^{-1} , deindustrialization - 220 mAh g^{-1}). This indicates that the electrode is characterized by low reversibility (about 57%). This generates a decrease in its capacity in the long run. The obtained results can be compared with literature data. The $\text{MoO}_3/\text{MoS}_2$ composite was synthesized. The authors note that the obtained system capacity (for 1C - 1100 mA g^{-1} , for C10 - 1200 mA g^{-1}) is greater than the individual components capacity (MoS_2 - 600 mAh g^{-1} , MoO_3 - 1000 mAh g^{-1}). The composition of the composite is 85% MoO_3 , 15% MoS_2 [23]. In the case of using MoS_2 obtained by hydrothermal method, the team of Chinese researchers received a large reversible capacity after the first cycle (for discharging - 1272 mAh g^{-1} , which is 3.4 times greater than for graphite, for charging - 801 mAh g^{-1}). The loss of reversibility was 37% [23]. For the $\text{MoS}_2/\text{graphite}$ composite (in the form of nanolayers) obtained in situ during the first operating cycle, the charging capacity was 2200 mAh g^{-1} , and for discharge - 1300 mAh g^{-1} , which is higher than the magnitudes of MoS_2 and graphite (nanolayers). After 50 cycles, the value of the discussed parameter was 1290 mAh g^{-1} (for comparison: pure molybdenum sulphide (IV) reached the capacity value equal to 605 mAh g^{-1}) [24].

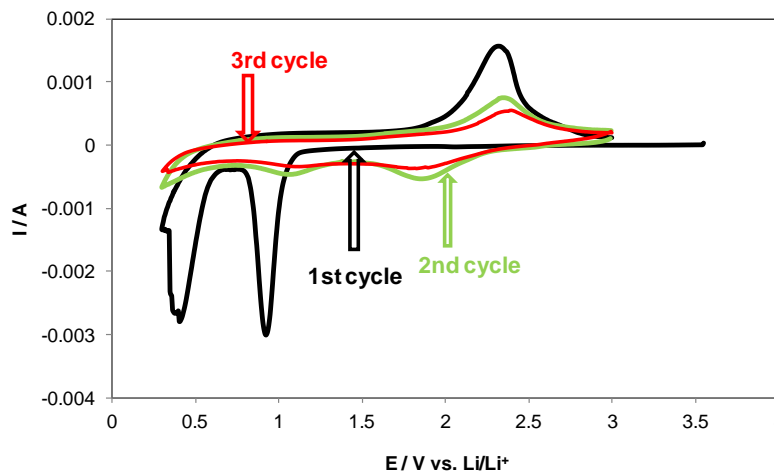


Figure 3. Cyclic voltammograms of the MoS₂|1M LiPF₆ in EC/DMC | Li (system) from the first to the third cycle at scan rate of 0.2 mV s⁻¹

The voltammogram shown in Figure 3 allows you to determine the electrode reactions that occurred at the electrode during the operation of the cell. In the first cycle, cathodic peaks occur near potential values of 0.4 V and 0.9 V. The first one is assigned the reaction of the Li_xMoS₂ con-version to the metallic Mo and Li₂S. This is described in reaction (1) [7]:



Behind the peak at 0.9 volts is the process of insertion of Li⁺ ions between the MoS₂ layers (formation of the Li_xMoS₂ system), which describes the equation (2) [7]:

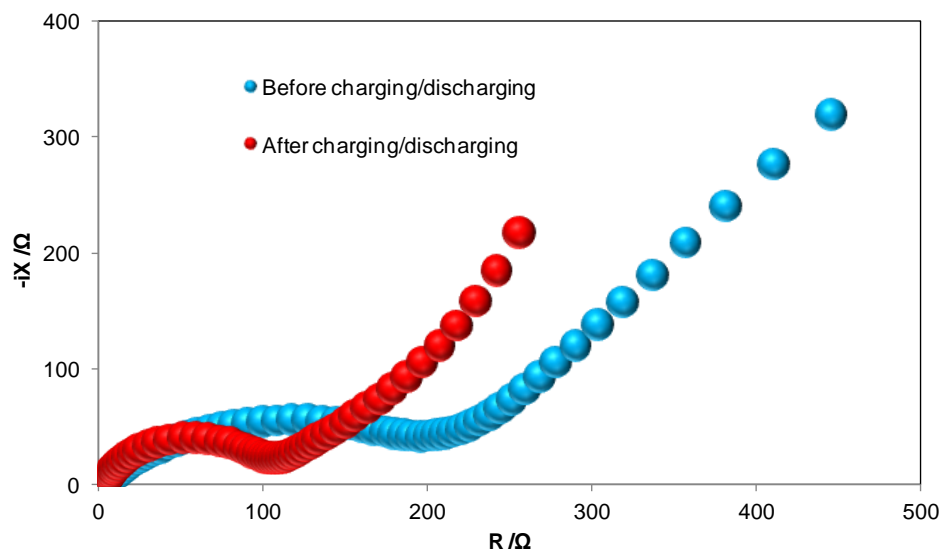


Figure 4. Electrochemical impedance spectra curie of MoS₂|1M LiPF₆ in EC/ DMC|Li (potential = 3.4 V).

In the second cycle, the peak from the lithium ion insertion disappeared, and the one at 0.9 V disappeared towards the higher potential values. It results from the fact that passing the current during

the voltammetric tests causes changes in the examined material. Molybdenum sulphide (IV) shows a short lifespan, which changes its behavior during the tests reveal itself after a small number of cycles. The anode peak for the first and the second cycle is revealed around a potential of about 2.4 volts. It is responsible for the oxidation reaction of Li_2S [2].

It is obvious that the resistance of the electrode before insertion of lithium ions into its structure is significantly higher than measured after the charging / discharging process. This is illustrated in the Nyquist graph shown in Figure 4.

The semicircle responsible for kinetics-controlled processes reaches the resistance of the order of 200 Ω . In addition, a very long diffusion tail of around 500 Ω is observed. Process resistance increased in the passive layer, but also in the load transfer process. Both loops are flattened and combined into one. A significant part of the impedance was revealed at low frequencies. The result is a straight inclined angle of more than 45 ° (the value of the ideal straight slope in the case of Warburg impedance, which is associated with diffusion). Warburg's high impedance testifies to the high contribution of diffusion to total electrode resistance.

Recently, MoS_2 nanostructures of various sizes, morphologies, and differentiation of the MoS_2 shape have been developed. This was to serve a wide range of application in LIBs, as well as to have a direct impact on the capacity obtained and the life span of such a link. For example, Tian et al. synthesized uniform small MoS_2 using a microwave method. The anode obtained showed a relatively large specific capacity of 1350 mAhg^{-1} (current density 0.5Ag^{-1}). The obtained structure of anode electrodes has a direct effect on limiting volume changes as well as on cycling stability, especially during Li^+ introduction and removal from MoS_2 layers.

To limit the change in volume and simultaneously reduce the path of lithium-ion diffusion and improve the measurement efficiency of anodic materials, different MoS_2 structures were used, such as microspheres, nanotubes or nanoparticles of MoS_2 as anode materials for LIBs [25-31].

3.2. The electrode based on $\text{MoS}_2/\text{TiO}_2$

The work of the obtained $\text{MoS}_2\text{-TiO}_2$ hybrids based on 100 cycles at a current density of 0.1 g cm^{-1} was presented. In numerous literature reports it can be read that these systems are characterized by low life expectancy due to the low conductivity of both oxides. The materials of this type obtained hydrothermal method are characterized by a great deal of structure and thus a significant limitation in the transport of electrons. Therefore, numerous studies are underway to improve the electrical conductivity of the $\text{MoS}_2\text{-TiO}_2$ hybrid, which seems to be necessary for the performance of such a lecture in a lithium-ion cell, especially during charge /discharge cycles at high currents.

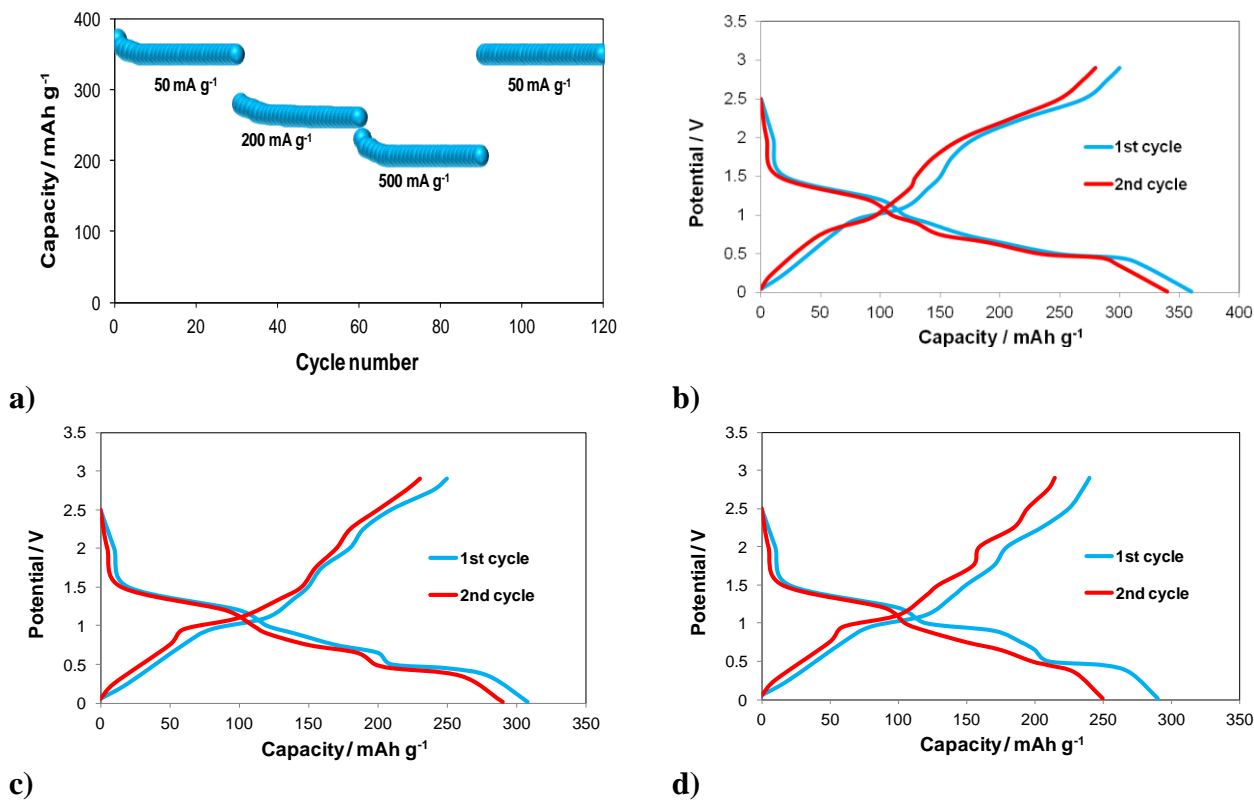


Figure 5. a) The rate capacity of MoS₂+5% weight SiO₂. Discharge-charge profiles of selected cycles at current density 50 mA g⁻¹ of: b) MoS₂+5% weight TiO₂|1M LiPF₆ in EC/DMC|Li; c) MoS₂+10% weight TiO₂|1M LiPF₆ in EC/DMC|Li; b) MoS₂+20% weight TiO₂|1M LiPF₆ in EC/DMC|Li.

It should be remembered that studying the kinetics of lithium ion transport is important in determining the performance of such a material. It also has a bearing on the number of charge/discharge cycles. It is also worth noting that in the majority of synthesized materials based on MoS₂ and TiO₂, molybdenum sulphide has direct contact with the electrolyte - its coating creates liquid/ solid phase boundaries [32-41].

Figure 5a shows the dependence of capacity on the number of cycles at variable current density. The chart shows that as the number of cycles increases with the current regime, the capacity drops. Its highest value, after the first cycle, at a current density of 5 mA g⁻¹, is about 380 mAh g⁻¹. The lowest, about 200 mAh g⁻¹, was obtained after the twentieth cycle of work. MoS₂ + 5% by weight TiO₂ behaves in a rather typical way - increasing the current density causes a decrease in capacity, with the difference that in the case of commercially used materials, this decrease is extended over time.

It can be noticed in Figure 5b that the capacity obtained after the first life cycle of the cell is lower than in the case of an electrode paste without an additive. The value was approximately 360 mAh g⁻¹. In the second cycle, in the insertion process, the capacity is estimated at approximately 345 mAh g⁻¹, which gives a reversibility of approximately 96%. Within one cycle the capacity value is not the same. This indicates the fact that the electrode is incompletely reversible with such a paste during a duty cycle of about 78% (for the first cycle: insertion - 360 mAh g⁻¹, deinsertion - 280 mAh g⁻¹). When we are dealing with 10% by weight addition of TiO₂, as seen in Figure 5c, there is a decrease in

capacity after the first insertion process (310 mAh g^{-1}) compared to the reference electrodes and doped at 5% by weight.

The capacity after the second charge is at 300 mAh g^{-1} , which gives a 97% reversibility. This indicates an improvement of this parameter in comparison with the previous variants. For the first cycle, for the deindication process, a capacity of about 255 mAh g^{-1} is obtained. Thanks to this, the reversibility, within one cycle, is 82%.

From Figure 5d it follows that 20% by weight addition of titanium oxide (IV) led to an even greater reduction in capacity after the first lithium ion insertion compared to smaller additions (first cycle: 295 mAh g^{-1} , second cycle: 250 mAh g^{-1}). This gives a reversibility of around 85%. This value is also the lowest when it is combined with other electrodes modified with titanium (IV) oxide. Within one cycle the capacity changes (for the first cycle): insertion - 295 mAh g^{-1} , deindustrialization - 225 mAh g^{-1} , which gives a reversibility of 76%. This is the lowest of three (for three different electrodes).

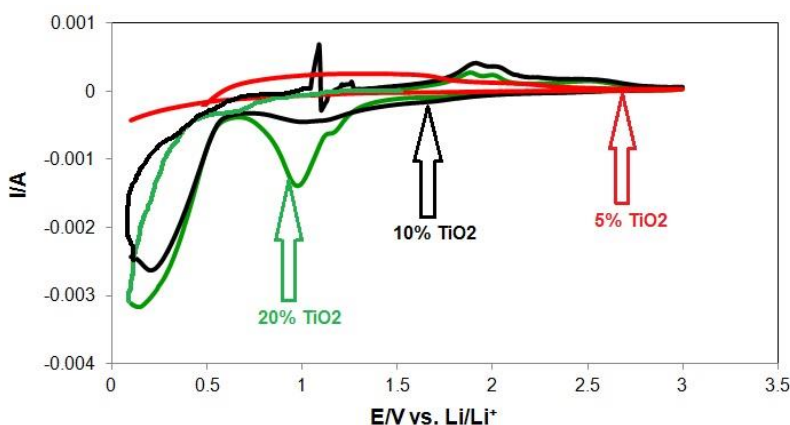


Figure 6. CV curves of the $\text{MoS}_2 + 5, 10, 20\%$ weight $\text{TiO}_2 | 1\text{M LiPF}_6$ in $\text{EC/DMC} | \text{Li}$. Scan rate: $0.2 \text{ mV} \cdot \text{s}^{-1}$, first scan.

In the case of the voltamperogram for TiO_2 modified electrodes (Fig. 6), only the curves for 10 and 20% by weight can be discussed. supplement. Both illustrate the behavior of the electrodes after the first cycle of work. Cathodic peaks at a potential of about 1 V correspond to the reaction of insertion of Li^+ ions, during which the MoS_2 structure changes from rhombohedral to octahedral. For cathodic peaks located in the vicinity of 1 V and 2.25 V, no equivalents were found in the publications that were the basis for the interpretation of the charts. Anode peaks occur around potentials of about 1.9 V and 2.1 V. They are assigned, probably the next, reactions: oxidation of Mo to MoS_2 and Li^+ to Li_xTiO_2 .

When using multilayer nanospheres formed from alternating layers of MoS_2 and carbon as the cathode material in a lithium-ion cell, electrochemical properties derive from a specific hierarchical structure, synergistic effect, and the occurrence of defects as additional active sites (introduced by roasting in 773 K under argon atmosphere). The results obtained (shown in Table 3) are most likely to be the result of a combination of faraday and non-free accumulation processes in the electrode material. Coulomb efficiency for the first and fifth charge/discharge cycles is 21.3 and 63.1 % for the current 0.3 C and 46.6 and 63.4 % for the 0.5 C current [3]. When dealing with MoS_2 layers located on

the surface of graphene (G) vertically, inter-phase interaction between C-O-Mo bonds can increase the electron transfer rate and the structural stability of the MoS₂/G electrode, which is very beneficial for Improving the performance and life cycle of the cell. Graphene layers contribute to improved composite electronic conductivity. At the same time they act not only as a material through which homogeneous dispersion of molybdenum sulphide nanoparticles (IV) is possible, but also as a buffer. It facilitates the reduction of the change in volume of electrode material generated during the life cycle of the cell [4].

Table 3. Capacitance values of MoS₂ electrodes without additives

Current	C / A kg ⁻¹	Capacities / Ah kg ⁻¹	Material	Electrode	Ref
0.1 C	700	3700	MoS ₂ /C multilayer nanospheres	cathode	[3]
		910	MoS ₂ nanobowls		
		642	MoS ₂ @C-400 nanobowls		
		988	MoS ₂ @C-500 nanobowls		
		1024	MoS ₂ @C-600 nanobowls		
0.2 C	670	850	MoS ₂ nanobowls	anode	[2]
		546	MoS ₂ @C-400 nanobowls		
		892	MoS ₂ @C-500 nanobowls		
		958	MoS ₂ @C-600 nanobowls		
0.3 C	700	1390	MoS ₂ /C multilayer nanospheres	cathode	[3]
		790			
0.5 C		660	MoS ₂ nanobowls		
		344	MoS ₂ @C-400 nanobowls		
		737	MoS ₂ @C-500 nanobowls		
		792	MoS ₂ @C-600 nanobowls		
		537	MoS ₂ nanobowls		
1 C		221	MoS ₂ @C-400 nanobowls		
		679	MoS ₂ @C-500 nanobowls		
		657	MoS ₂ @C-600 nanobowls		
		270	MoS ₂ nanobowls		
2 C	670	141	MoS ₂ @C-400 nanobowls	anode	[2]
		482	MoS ₂ @C-500 nanobowls		
		504	MoS ₂ @C-600 nanobowls		
		99	MoS ₂ nanobowls		
5 C		69	MoS ₂ @C-400 nanobowls		
		353	MoS ₂ @C-500 nanobowls		
		363	MoS ₂ @C-600 nanobowls		
10 C		5	MoS ₂ nanobowls		
		67	MoS ₂ @C-400 nanobowls		
		185	MoS ₂ @C-500 nanobowls		
		171	MoS ₂ @C-600 nanobowls		
100 A kg ⁻¹		1077	MoS ₂ multilayer graphene nanospheres		[4]
		907			
1000 A kg ⁻¹	-	14	MoS ₂		[5]
		192	MoS ₂ /graphene (1:1) - composite aerogels		
		348	MoS ₂ /grafen (0.5:1) - composite aerogels		
		250	MoS ₂ /graphene (0.25:1) - composite aerogels		

TiO₂ is an amphoteric oxide. It reacts with concentrated sulfuric acid (VI) to give titanyl sulfate, and when it is melted with hydroxides, carbonates or oxides of other metals, it forms titanates.

It is also characterized by high mechanical resistance and photochemical stability [6]. When dealing with core-shell composites formed with TiO₂ together with the MoS₂ nanolayers by hydrothermal method, where one of the substrates is cetyltrimethylammonium bromide, they have better electrochemical properties than pure molybdenum (IV) sulphide. Then we have to deal with a higher specific capacity and reversibility during the cyclic operation of the cell. This may result from the dispersion of sulphide nanowires on the surface of the oxide, which accelerates surface electrode reactions and ensures structural stability. In addition, the TiO₂ nanospheres themselves act as stabilizers of the MoS₂ structure after many cycles of the system [7].

In the case of using the synthesized TiO₂@MoS₂/C system as the electrode paste, an improvement in the electrochemical properties is also obtained as compared to the unmodified molybdenum (IV) sulphide. This is due to the fact that the presence of oxide plates improves cycle speed and efficiency. Thanks to the scaffolding in the form of titanium oxide (IV), MoS₂/C, it has the ability to attach to it, which prevents the phenomenon of exfoliation of molybdenum sulphide (IV) from becoming quite common [8].

Table 4 presents literature data describing the value of the specific capacitance of the electrode depending on the material used in the preparation of the electrode paste

Table 4. Capacity for electrodes with TiO₂

Current / A·kg ⁻¹	Capacity / Ah·kg ⁻¹	Material	Ref
100	643	TiO ₂ @MoS ₂ /C spheres	[8]
	467	TiO ₂ @MoS ₂ TiO ₂ -nanospheres, MoS ₂ -nanospheres	[7]
	750	C@MoS ₂	[9]
	400	MoS ₂ supported on carbon nanotubes	[10]
	947	3D flower-like MoS ₂ spheres	[11]
	982	MoS ₂ /C nanospheres - in foam-like carbon sheets	[12]

3.3. The electrode based on MoS₂/SiO₂

The graph below (Figure 7a) shows the capacitance values in relation to the number of cycles performed, using different current regimes, for MoS₂ doped with 5% by weight. SiO₂. As you can see, the system performed 20 cycles with an initial capacity of 310 mAh g⁻¹, which gradually decreased with each increase in the current density. Finally at 50 mAh g⁻¹ is about 42% lower (180 mAh g⁻¹).

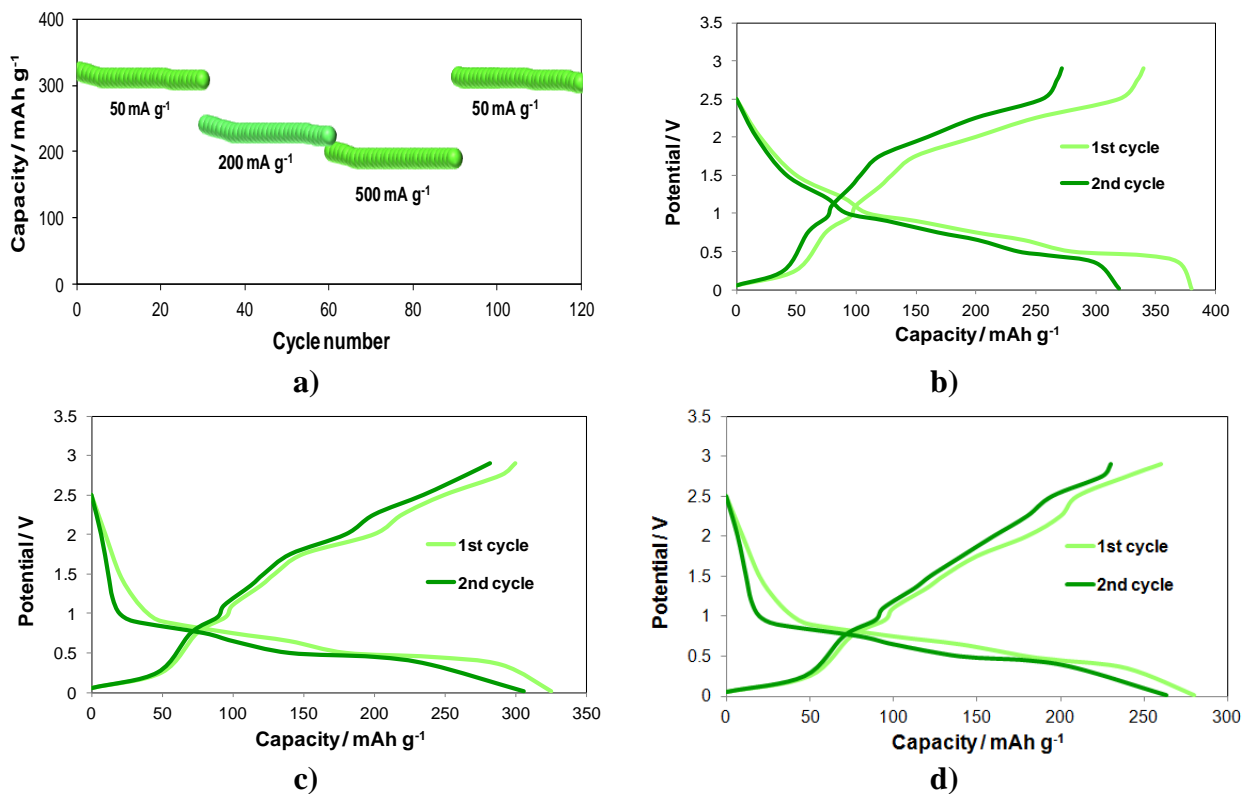


Figure 7. a) The rate capacity of MoS₂+5% weight SiO₂. Discharge-charge profiles of selected cycles at current density 50 mA g⁻¹ of: b) MoS₂+5% weight SiO₂|1M LiPF₆ in EC/DMC|Li; c) MoS₂+10% weight SiO₂|1M LiPF₆ in EC/DMC|Li; d) MoS₂+20% weight SiO₂|1M LiPF₆ in EC/DMC|Li.

Figure 7b shows the constant-current charge / discharge curves for an anode containing 5% by weight SiO₂ for the first two cycles. For the first lithium ion insertion into the anode structure (charging curve), the cell's capacity is approximately 380 mAh g⁻¹. On the second charge this capacity is reduced by about 10% and is 340 mAh g⁻¹.

The curves shown in Figure 7c were created by examining a cell with an anode containing 10% by weight SiO₂. In this case the 1 cycle capacity is lower than for a 5 wt% system. SiO₂ is approximately 325 mAh g⁻¹. With the second lithium ion insertion, it decreases only by 0.6% and is 310 mAh g⁻¹.

For a cell with an anode containing 20% by weight SiO₂ (Fig. 7d) the capacity achieved during loading/unloading is the lowest of those presented so far. For charging during the first cycle, the capacity is approximately 280 mAh g⁻¹, and for the second 270 mAh g⁻¹. This difference is negligible. In studies of new electrode materials that are synthesized, attainable properties are determined by the type of additive.

For example, the very thin MoS₂/chitosan-assisted graphs produced after the first lithium ion insertion have a capacity of 988 mAh g⁻¹ (charging) and 1432 mAh g⁻¹ (discharge) - reversibility 69% [42]. Another example is the hybrid MoS₂/polyaniline composite (MoS₂/PANI), the capacity of which during the first charging is 910 mAh g⁻¹, and discharge is 1148 mAh g⁻¹ [43]. In turn, for the electrode

material MoS₂/rGO, which is synthesized in the presence of SiO₂ capacity of the charging process 1260.5 mAh g⁻¹, and discharging 2279 mAh g⁻¹ [43].

In addition, environmentally friendly and low cost carbon nanostructures MoS₂/carbon fibers (MoS₂/SFTC) have been prepared by an easy hydrothermal method. They showed the reversible specific capacity of 437.2 mAh g⁻¹ is supported after 50 cycles at a current density of 50 mA g⁻¹ (even at high current density of 2000 mA g⁻¹, the reversible specific capacity could be supported at 241.1 mAh g⁻¹)[44].

The efficient use of titanium dioxide in photoelectrochemistry is limited by the high value of the forbidden gap of TiO₂ ($E_g = 3.0-3.4$ eV). Heterocomponents consisting of semiconductors significantly differing in the electronic structure allow for extending the range of light absorption and increasing the recombination time. The formation of TiO₂-based composites-based materials enjoys growing interest. rGO, the oxidised form of graphene, appears to be an interesting material for forming bonds with semiconductors and metals, and the layered MoS₂ has an electronic structure that allows its use as a component of the photo-water decomposition in the PEC (PhotoElectrochemical Cell). The aim of the work was to examine the effect of the addition of rGO and MoS₂, deposited under various conditions on the properties of TiO₂-based photoanodes. In the presented work, rGO was synthesized by the modified Hummers method and MoS₂ by the hydrothermal method, then deposited on the surface of TiO₂ (nanotubes or continuous layer) electrochemically (rGO, MoS₂) and hydrothermal (MoS₂).

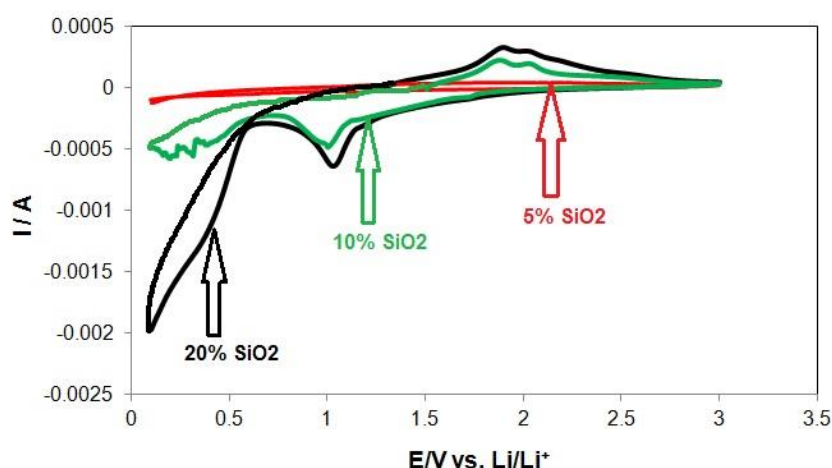


Figure 8. CV curves of the MoS₂+ 5, 10, 20% weight SiO₂| 1M LiPF₆ in EC/DMC|Li. Scan rate: 0.2 mV·s⁻¹, first scan.

Cyclic voltammogram (Fig. 8) shows the results of measurements of three electrodes. During reduction, one peak is visible at a potential of about 1 volt, it is responsible for the insertion reaction. In turn, the next two occur at the potentials of 1.8 V and 2.1 V. Ne they are completely separated, which indicates that the deindration of lithium was two-stage. This is also seen in Figure 8 due to the double plate (20 wt% SiO₂).

In summary we can thought that on basis of above analyses and evidences, the MoS₂/TiO₂ or SiO₂ shows significantly enhanced cycling stability and rate capability compared with pure MoS₂, which can be attributed to their favorable structural advantages (Fig. 9): the abundant mesopores and defect-rich, interlayer-expanded, and few-layered MoS₂ facilitate the Li-ion diffusion across the electrode and active material, respectively [45].

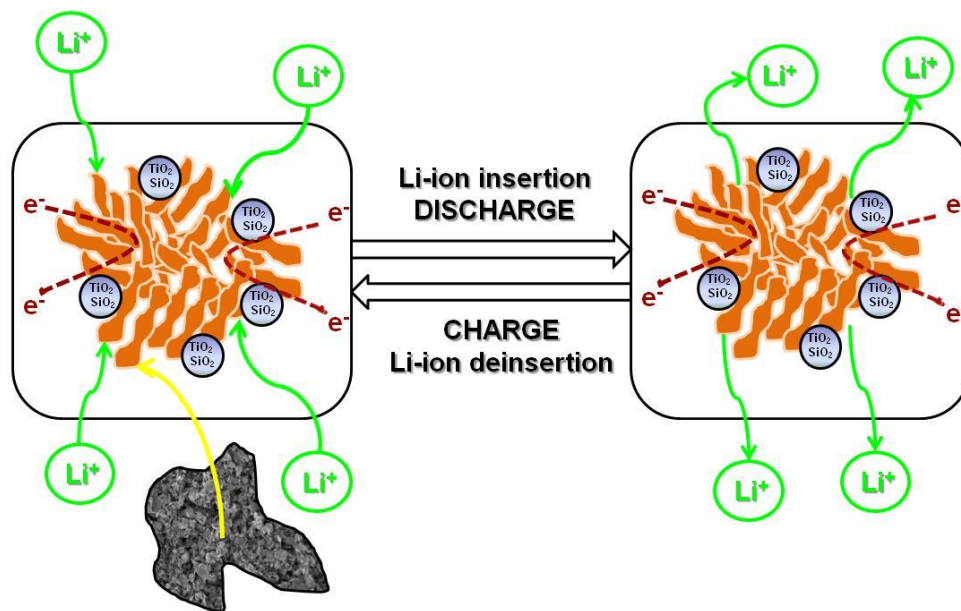


Figure 9. Schema of MoS₂/SiO₂ or TiO₂ anode material during the charge/discharge processes.

Moreover the continuous porous structure can provide sufficient void space to buffer the mechanical stress arising from the volume variation upon Li-ion insertion/deinsertion, resulting in a robust architecture.

Table 5. Comparison of mean capacitance values for galvanostatic charging/discharging and reversibility during cyclic operation of the electrodes tested.

Materials	Capacity / mAh g ⁻¹		Reversibility / %
	Charge	Discharge	
MoS ₂	368	210	57
MoS ₂ +5%(wt./wt.)TiO ₂	353	270	77
MoS ₂ +10%(wt./wt.)TiO ₂	305	250	82
MoS ₂ +20%(wt./wt.)TiO ₂	273	240	88
MoS ₂ +5%(wt./wt.)SiO ₂	360	300	83
MoS ₂ +10%(wt./wt.)SiO ₂	318	280	88
MoS ₂ +20%(wt./wt.)SiO ₂	275	245	89

Data of this paper are presented in Table 5. In summary, molybdenum sulfide can be considered as a potential electrode material for lithium-ion cells. By using additives, better reversible

values are obtained, which is a signal that further research on MoS₂ in different systems can produce satisfactory results.

4. CONCLUSIONS

Molybdenum disulphide has been widely used in many branches of industry due to its properties. It is used as various types of coating, increasing resistance to load, friction and corrosion. It has been successfully used for the production of catalysts involved in the processes: HDS, HER and the synthesis of mixed alcohols. It also has properties thanks to which it can become an important material in the broadly understood field of optoelectronics electronics, or as an electrode material.

Experimental studies have shown that MoS₂ nanoparticles have catalytic properties that can be used in the electrocatalytic production of hydrogen. The activity of molybdenum disulfide nanoparticles can be increased by doping with cobalt. Numerous research works indicated that the formed hybrids of MoS₂, tungsten monocarbide and graphene oxide were characterized by large surface area, increased conductivity and excellent catalytic activity in the HER reaction.

The aim of the study was to investigate molybdenum sulphide as a potential electrolyte material used in lithium-ion cells and to improve its electrochemical properties. The most commonly used anode was graphite. MoS₂ has a higher capacity than graphite (~372 mAh g⁻¹) by about 180%. The problem, however, is its short life span (up to 20 work cycles). The voltammogram for the reference electrodes, on which it can be clearly seen that with each successive work cycle there is a flattening of the peaks. This demonstrates the fact that the electrode material has been depleted. Additives were used to improve electrochemical properties of molybdenum sulphide (IV).

Analysis of comparative electrodes (MoS₂ without additives) was started from the electrochemical studies of impedance spectroscopy. As a result, they learned their resistance before the first and subsequent work cycles. Values have decreased. This is due to the formation of the passive layer of the SEI (Solid Electrolyte Interphase) on the surface of the electrode. The mechanism of their reduction is that after the formation of the lithium ion, the reaction of "embedding" lithium ions is favored because the surface of the electrode is isolated from the electrolyte by a layer of insoluble compounds, eg. lithium alkyl carbonate (CH₂OCO₂Li)₂, which is the decomposition product EC.

Taking into account the electrode capacitance at the galvanostatic storage, the best results were achieved using pure molybdenum sulphide. No add-on did not increase the capacity. Within one additive, as it increased its mass share, capacity decreased. With galvanostatic discharge, the highest capacity was obtained for an anode with 5 wt% SiO₂. By comparing the corresponding electrodes with two different additives, silicon oxide (IV) doped in each case exhibited better capacities than their counterparts with titanium oxide (IV). Advantages of reversible values have been obtained during cyclic operation of the cell. Each additive increased the size of the parameter in question relative to the reference electrodes. Increasing the share of the additive caused an increase in reversibility. The best results were obtained for doping with silicon oxide (IV).

The results indicate that the structure provides active sites for the storage of lithium ions, facilitates fast transport of lithium ions and electrons. The aggregation of MoS₂ particles during lithiation/delithiation processes, is led to the high specific capacity and rate capability.

ACKNOWLEDGEMENTS

Support of grant 03/31/DSPB/0335 is gratefully acknowledged.

References

1. B. Peng, J. Chen, *Coordination Chemistry Reviews*, 253 (2009) 2805.
2. C. Cui, X. Li, Z. Hu, J. Xu, H. Liu, J. Ma, *Royal Society of Chemistry*, 5 (2015) 92506.
3. O.L. Shyyko, O.V. Kotsyubynsky, M.I. Budzulyak, P. Sagan, *Nanoscale Research Letters*, 11-243 (2016) 1.
4. Y. Teng, H. Zhao, Z. Zhang, Z. Li, Q. Xia, Y. Zhang, L. Zhao, X. Du, Z. Du, P. Lv, K. Świerczek *American Chemical Society Nano*, 10 (2016) 8526.
5. T. Zhang, I. Kong, M. Liu, Y. Dai, K. Yan, B. Hu, *Materials nad Design*, 112 (2018) 86.
6. J. Cho, C.S. Kim, S.I. Yoo, *Electrochemical Solid-State Letters*, 3 (2000) 362.
7. B. Zhao, Z. Wang, Y. Gao, L. Chen, M. Lu, Z. Jiao, Y. Jiang, Y. Ding, L. Cheng, *Applied of Surface Science*, 390 (2016) 209.
8. G. Li, L. Yu, H. Hu, Q. Zhu, Y. Wang, Y. Yu, *Electrochimica Acta*, 212 (2016) 59.
9. L. Zhang, X.W. Lou, *Chemistry European Journal*, 20 (2014) 5219.
10. Q. Wang, J.H. Li, *The Journal of Physichal Chemistry, C* 111 (2007) 1675.
11. T. Yang, Y.J. Chen, B.H. Qu, L. Mei, D. Lei, H.N. Zhang, Q.H. Li, T.H. Wang, *Electrochimica Acta*, 115 (2014) 165.
12. B.B. Wang, Y. Xia, G. Wang, Y.X. Zhou, H. Wang, *Chemistry European Journal*, 309 (2017) 417.
13. K.-X. Wang, X.-H. Li, J.-S. Chen, *Advance of Materials*, 27 (2015) 527.
14. Shu H, Li F, Hu C, Liang P, Cao D, X. Chen, *Nanoscale*, 8 (2016) 2918-2926.
15. Z. Zeng, X. Zhang, K. Bustillo, K. Niu, C. Gammer, J. Xu, H. Zheng, *Nano Letters*, 15 (2015) 5214.
16. B. Kurc, *International Journal of Electrochemistry Science*, 13 (6) (2018) 5938.
17. B. Kurc *Journal Solid State of the Electrochemistry*, 16 (2014) 673.
18. R. Tenne, L. Margulis, M. Genut, G. Hodes, *Nature*, 360 (1992) 444.
19. H.S.S. Ramakrishna Matte, A. Gomathi, A.K. Manna, D.J. Late, R. Datta, S.K Pati, C.N.R. Rao *Angewandte Chemie International Edition*, 49 (2010) 4059.
20. R.R. Haering, J.A.R. Stiles, K. Brandt, US Patent, 1980, No. 4224390.
21. X. Chen, Z. Chen, J. Li, *Chinese Science Bulletin*, 58 (2013) 1632.
22. F. Xiong, H. Wang, X. Liu, J. Sun, M. Brongersma, E. Pop, Y. Cui, *Nano Letters*, 15 (2015) 6777.
23. G. Guo, J. Hong, C. Cong, X. Zhou, *Journal of Materials Science*, 40 (2005) 2557.
24. J. Zhao, H. Ren, C. Gu, W. Guan, X. Song, *Journal Alloys of Compounds*, 781 (2019) 174.
25. Z.Y. Zhang, S.L. Wu, J.Y. Cheng, W.J. Zhang, *Energy Storage Materials*, 15 (2018) 65.
26. X.H. Tian, Q.M. Gao, H. Zhang, Z.Y. Li, H. Xiao, Q. Zhang, L. Ma, *Nanoscale*, 10 (2018) 5222.
27. Y.C. Jiao, A.M. Hafez, D.X. Cao, A. Mukhopadhyay, Y. Ma, H.L. Zhu, *Small*, 14 (2018) 1.
28. L. Vieira, J.R.M. Neto, O.P. Ferreira, R.M. Torresi, S.I.C. Torresi, O.L. Alves, *RSC Advances*, 8 (2018) 30346.
29. X.D. Zheng, Y.L. Zhu, Y.L. Sun, Q.J. Jiao, *J. Power Sources* 395 (2018) 318.
30. K. Xie, Z.H. Liu, Y.R. Wang, G.S. Song, S.Q. Cheng, *New J. Chem.* 42 (2018) 10935.

31. Y.C. Jiao, A. Mukhopadhyay, Y. Ma, L. Yang, A.M. Hafez, H.L. Zhu, *Advances of Energy Materials*, 8 (2018) 1.
32. M. Mao, L. Mei, D. Guo, L. Wu, D. Zhang, Q. Li, T. Wang, *Nanoscale*, 6 (2014) 12350.
33. B. Guo, K. Yu, H. Fu, Q. Hua, R. Qi, H. Li, H. Song, S. Guo, Z. Zhu, *Journal of Materials Chemistry A*, 3 (2015) 6392.
34. J.-Y Liao, B.D. Luna, A. Manthiram, *Journal of Materials Chemistry A*, 4 (2014) 801-806.
35. R. Dai, A. Zhang, Z. Pan, A.M. Al-Enizi, A.A. Elzatahry, L. Hu, G. Zheng, *Small*, 12 (2016) 2792.
36. W. Xu, T. Wang, Y. Yu, S. Wang, *Journal of Alloys Compounds*, 689 (2016) 460.
37. G. Li, L. Yu, H. Hu, Q. Zhu, Y. Wang, Y. Yu, *Electrochimica Acta*, 212 (2016) 59.
38. X. Xu, Z. Fan, S. Ding, D. Yu, Y. Du, *Nanoscale*, 6 (2014) 5245.
39. X. Li, W. Li, M. Li, P. Cui, D. Chen, T. Gengenbach, L. Chu, H. Liu, G. Song, *Journal of Materials Chemistry A*, 3 (2015) 2762.
40. B. Chen, N. Zhao, L. Guo, F. He, C. Shi, C. He, J. Li, E. Liu, *Nanoscale*, 7 (2015) 12895.
41. B. Chen, E. Liu, F. He, C. Shi, C. He, J. Li, N. Zhao, *Nano Energy*, 26 (2016) 541.
42. M. Lin, Z. Xiaoping, X. Limei, X. Xuyao, Z. Lingling, C. Weixiang, *Electrochimica Acta* 167 (2015) 39.
43. Y. Lin, T. Su, *Applied Surface Science*, 387 (2016) 661.
44. Y. Liu, A. Qin, S. Chen, L. Liao, K. Zhang, Z. Mo, *International Journal of Electrochemistry Science*, 13 (2018) 2054.
45. B. Chen, H. Lu, N. Zhao, C. Shi, E. Liu, C He, L Ma, *Journal of Power Sources* 387 (2018) 16.

© 2019 The Authors. Published by ESG (www.electrochemsci.org). This article is an open access article distributed under the terms and conditions of the Creative Commons Attribution license (<http://creativecommons.org/licenses/by/4.0/>).